IV. ELECTRICAL PROPERTIES OF GROWN LAYERS AND IMPURITY DOPING

1. Introduction

In this chapter, electrical properties of undoped 3C-SiC grown on Si are first mentioned. Characterization by Hall measurements, observation of EBIC(electron beam induced current) images and formation of Schottky barriers were carried out. Before the success of growth on Si by the combination of the carbonization and CVD growth, such evaluation of electrical properties was very difficult because of a small size of a crystal.

Acceptor doping of B and Al is also mentioned in this chapter. Since undoped crystals of SiC were usually n-type, acceptor doping was necessary for the fabrication of p-n junctions and active devices. III_b elements such as B, Al and Ga work as acceptors in SiC. Their activation energies in 3C-SiC were obtained by photoluminescence observation as 735[1], 254[2] and 343meV[3] for B, Al and Ga, respectively. The values of these activation energies are rather high. The ionization energies of P and As donors and a B acceptor in Si are 44, 49 and 45meV[4]. A deep activation energy will give rise to rapid increase of carrier concentration by raising temperature. Though Al has the most shallow level as an acceptor in 3C-SiC, doping of Al during CVD growth involves some technical difficulties. Because it does not have any gaseous compounds at room temperature. B has gaseous compounds for examples B_2H_6, BF_3 and BCl_3. In this work B_2H_6 and organic Al was used for p-type doping. Used organic Al's were TMA(trimethyl-aluminum) and TEA(triethyl-aluminum) which are liquid at room temperature. By a bubbling method using H_2 organic Al was introduced. The influence of doping on grown layers and electrical properties of doped layers is mentioned.

Note: In this and the following chapters (100) well oriented Si substrates and Si substrates oriented *n*° off (100) towards (011)

are called as (100) substrates and *n*° off substrates, respectively. Where *n* is 2, 4 or 6.

2. Electrical properties of undoped layers

2-1. Hall measurement

In this section electrical properties of undoped layers on both (100) and off substrates are mentioned. All undoped layers showed n-type conduction in Hall measurements as far as measurements were carried out.

(Grown layers on (100) substrates)

Figure 1 shows the relationship between electron mobilities and electron concentrations of undoped grown layers on (100) substrates. The grown layers contained APD's. Hall measurements were carried out by van der Pauw method. Si substrates were removed by a mixed solution of HNO_3 and HF before the measurement to avoid the errors due to current conduction through the substrates. The maximum electron mobility on (100) substrates was $488cm^2/Vs$ at a carrier concentration of $3.18x10^{16}cm^{-3}$. The thickness of this sample was about 5μm. Though all the samples in Fig.1 were undoped, the carrier concentration changed in the range of 10^{16}-$10^{19}cm^{-3}$. The undoped carrier concentration was usually lower than $2x10^{17}cm^{-3}$. The most probable origin of high carrier concentrations was impurities in H_2 carrier gas. Because, most of the samples which showed very high carrier concentrations were grown without a H_2 purifier. However, sudden increase up to about $1x10^{18}cm^{-3}$ was rarely observed. The origin of this phenomenon is not clear. The lowest resistivity unintentionally obtained was 0.0015Ωcm. This fact means that by an appropriate doping low resistive layers which are necessary for good ohmic contacts are easily obtainable. When a H_2 purifier was used, a typical carrier concentration was in the range of $3x10^{16}$-$2x10^{17}cm^{-3}$.

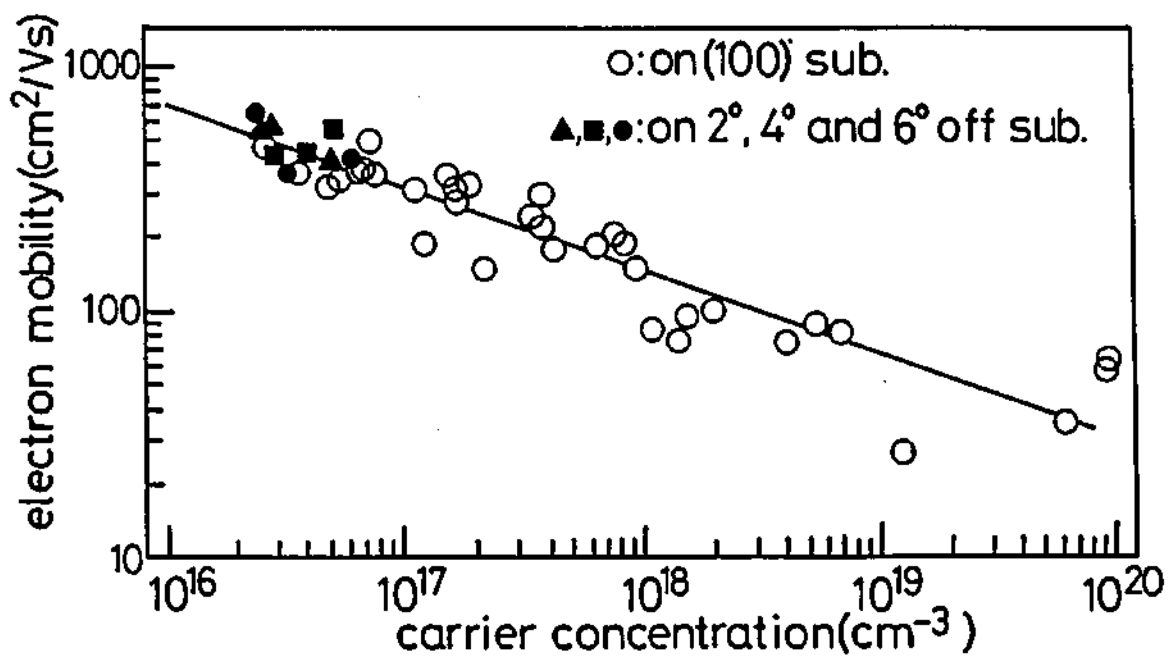

Fig.1 Relationship between electron mobilities and carrier concentrations of undoped grown layers. White circles and solid symbols represent grown layers on (100) and off substrates, respectively.

Recently Suzuki et al.[5] reported that nitrogen was detected by ESR(electron spin resonance) and SIMS(secondary ion mass spectroscopy) measurements for undoped grown layers. The amounts of nitrogen estimated from the ESR measurement were proportional to carrier concentrations. This is a noteworthy report though they added a comment that without a further investigation the residual impurity cannot be asserted to be nitrogen.

(Grown layers on off substrates)

The grown layers on off substrates showed electrical anisotropy, as explained below. In van der Pauw measurement using such a specimens as Fig.2, a value of R is defined by the following formulas.

$$r_{34}=V_{34}/I_{21}, \quad r_{41}=V_{41}/I_{32} , \tag{1}$$

$$R \equiv r_{34}/r_{41} \text{ or } r_{41}/r_{34} \quad (R>=1) , \tag{2}$$

where V_{mn} and I_{mn} are voltage and current between electrodes m and n(m,n: integer, $1 \leq m,n \leq 4$). If the sample is exactly square and isotropic and electrodes are located symmetrically, R should be 1.0. When the grown layers on (100) substrates were measured, R was close to 1.0 as long as the samples were nearly square. However, when the grown layers on off substrates were used, the value of R was rather larger than 1.0. Such a result was considered to originate from electrical anisotropy. Based on results of van der Pauw measurement, the relationship between anisotropy and off orientation or wedge-like surface morphology was obtained as shown in Fig.3. When currents flow in parallel to the wedges, the grown layers showed lower resistivity. This direction is defined as the parallel direction. For the perpendicular direction higher resistivity was obtained. van der Pauw method is not suitable for samples with anisotropy. And so the standard Hall measurement was carried out. Bridge type specimens which have a complex shape as shown in Fig.4(a) are usually utilized for the standard Hall measurement. However, thin SiC films whose substrates were removed are too fragile to be cut into such a shape. Therefore, Hall measurements were carried out

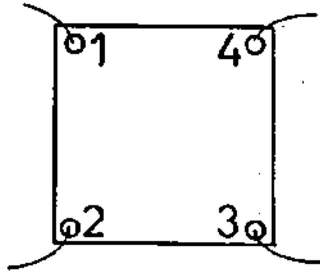

Fig.2 Specimen for van der Pauw measurement.

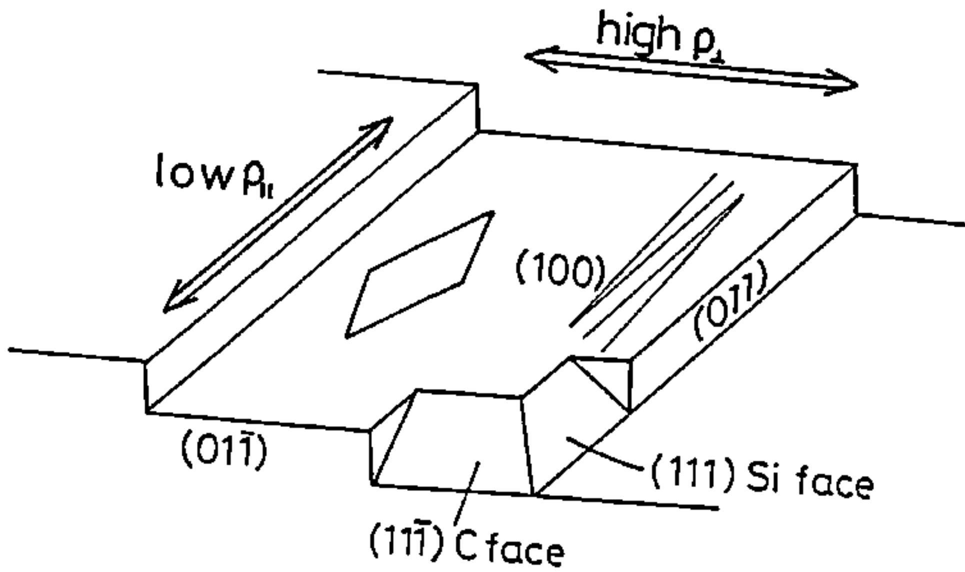

Fig.3 Directional relationship between the electric anisotropy and off orientation of substrates.

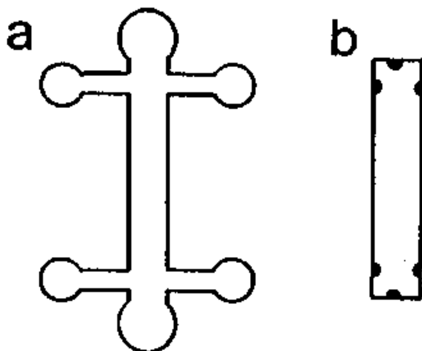

Fig.4 Shapes of specimens for Hall measurement. (a)Standard "bridge-type" and (b)used one for this investigation.

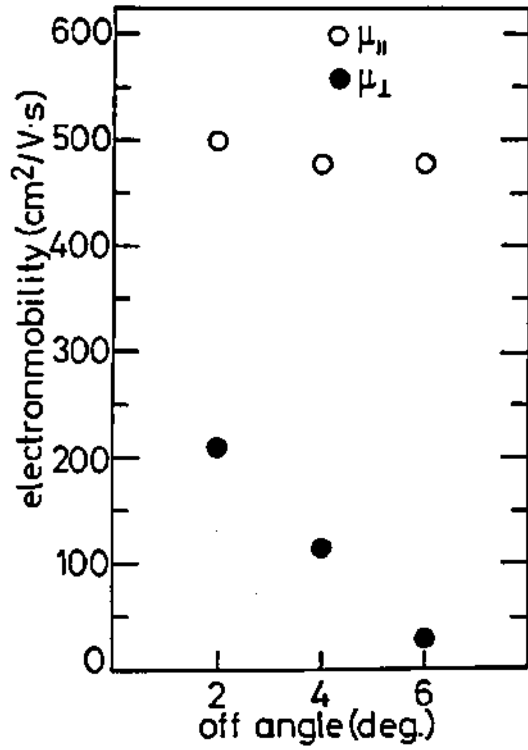

Fig.5 Electron mobility as a function of off angle.

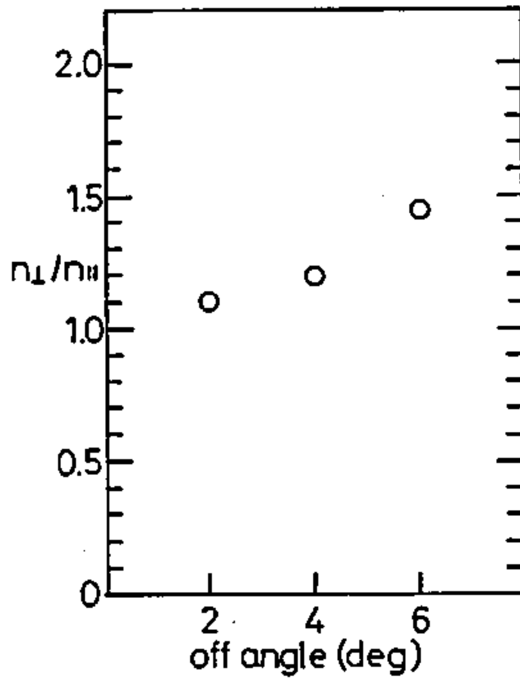

Fig.6 Ratio of $n_{\perp}$ and $n_{\parallel}$ as a function of off angle.

using the specimens which has a shape like Fig.4(b). The grown layers on the 2°, 4° and 6° off substrates were used. The thicknesses of the samples were 8-24μm. Figure 5 shows electron mobilities of the parallel and perpendicular directions. The horizontal axis of Fig.5 represents off angles of substrates. An average value of three samples were used as the electron mobility for each off angle. The electron mobility of the parallel direction($\mu_{\parallel}$) was independent of the off angle and its values were constantly about 500cm^2/Vs. However, the electron mobility of the perpendicular direction($\mu_{\perp}$) reduced as the off angle of the substrates became larger. Even at an off angle of 2°, $\mu_{\perp}$ was about half of $\mu_{\parallel}$. The electron concentrations of these samples were about 3-5x10^{16}cm^{-3}. The obtained maximum electron mobility was 650cm^2/Vs with a carrier concentration of 2.4x10^{16}cm^{-3}. The correlation between $\mu_{\parallel}$ and $n_{\parallel}$ on the off substrates are plotted in Fig.1 by solid symbols. Their correlation was similar to that for (100) substrates. Therefore, the improvement of electron mobility by the elimination of APD's was not observed. $\mu_{\perp}$ and $n_{\perp}$ showed no meaningful correlation. Figure 6 shows the ratio made by $n_{\perp}$ and $n_{\parallel}$. When the off angle was 2°, the ratio was close to 1.0. However, as the off angle increased, the ratio increased. It is not clear whether the observed anisotropy in the carrier concentration was due to some problems in measurements or not. Further characterization using a bridge type specimen shown in Fig.4(a) is expected.

2-2. EBIC observation

EBIC observation was carried out using Au-SiC Schottky barriers. Characteristics of the Schottky barriers are mentioned in the next section. Figures 7(a) and (b) show SEM(scanning electron microscope) and EBIC images of the grown layers on (100) substrates, respectively. The surface of the sample was ethced in molten KOH to visualize APB's as grooves. In the EBIC image of Fig.7(b) a random black and white pattern was observed, which indicates the existence of high-density recombination

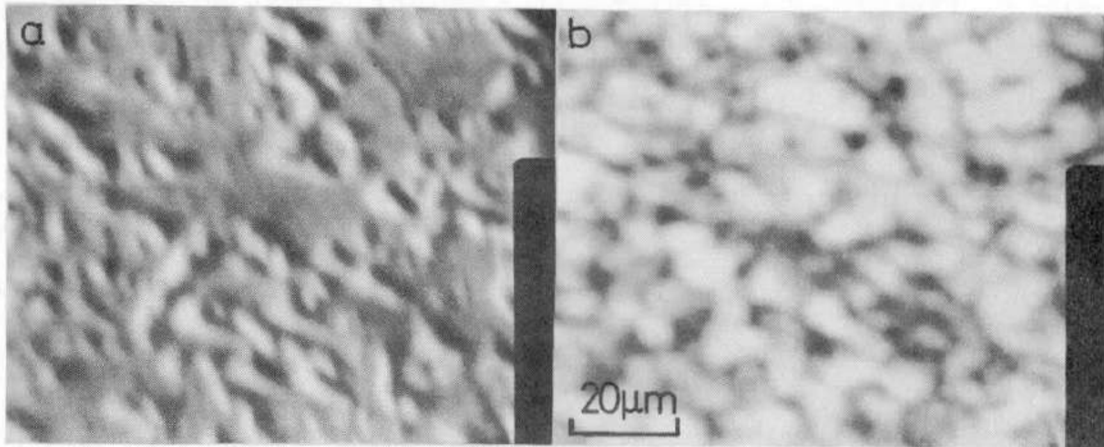

Fig.7 (a)SEM and (b)EBIC images of a grown layer on a (100) substrate. Surface of the sample was etched with molten KOH and APB's are observed as grooves.

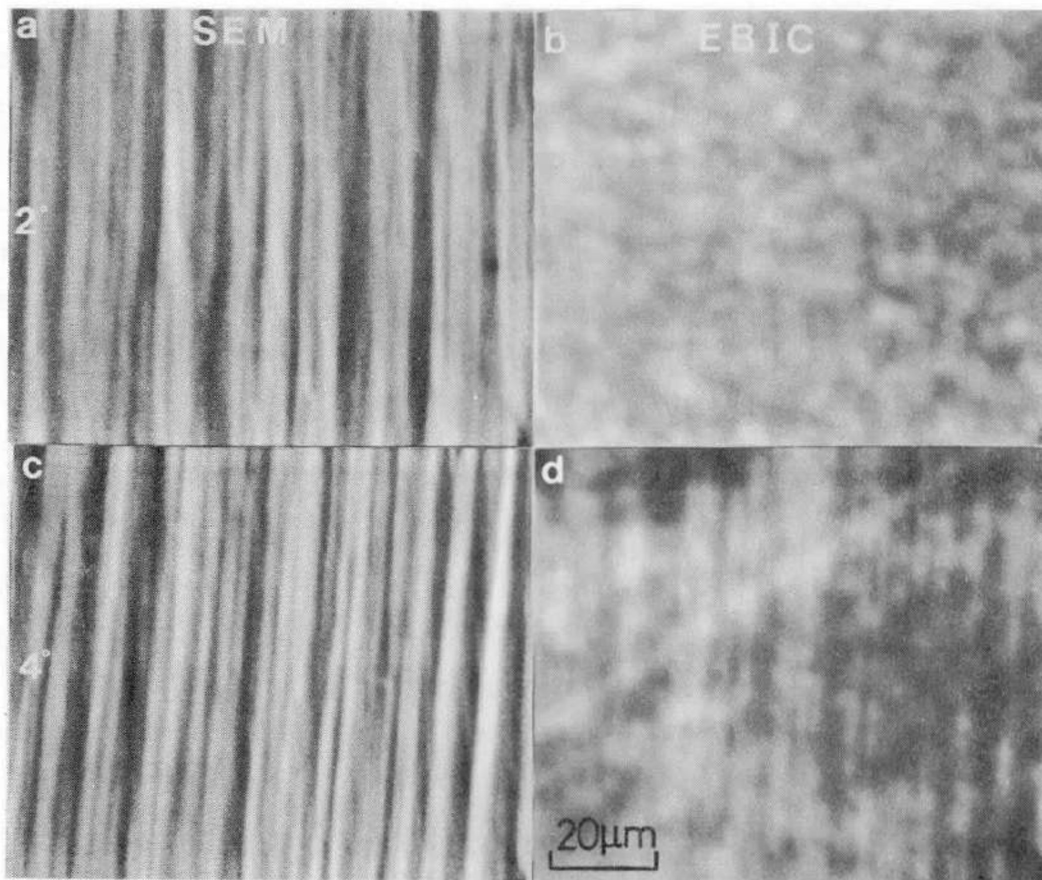

Fig.8 SEM and EBIC images of grown layers on off substrates.

centers. By comparing this EBIC image with its SEM image, the following two features were noticed. (1)The distribution pattern of grooves in the SEM image is similar to that of black lines in the EBIC image. (2)In the EBIC image there are many black parts which have no correspondent grooves in the SEM image. To sum up these two features, there are two types of recombination centers related and unrelated to APB's.

Figures 8(a)-(d) show SEM and EBIC images of the grown layers on the 2° and 4° off substrates. Grown layers on both the 2° and 4° off substrates showed similar surface morphology which consists of wedge patterns. The EBIC images showed different features due to the off angle. The EBIC image for the 2° off substrate in Fig.8(b) showed a random black and white pattern. However, the EBIC image for the 4° off substrate showed black lines in addition to a random pattern. These black lines point the same direction as a wedge-like morphology. The random black and white pattern observed for the 2° off substrates means that there exist recombination centers unrelated to APB. The black lines observed for the 4° off substrates indicate that the introduction of the off orientation with a large off angle gave rise to novel recombination centers. The black lines point the parallel direction defined in the previous section. The recombination centers observed as the black lines are considered to have some relation with the anisotropy mentioned in the previous section. The relationship between the recombination centers observed as the black lines and crystal defects is not clear. To discuss from a crystallographical standpoint characterization to observe crystal defects e.g. TEM (transmission electron microscope) should be utilized.

2-3. Schottky barrier

Au is the most popular metal to form Schottky barriers with n-type SiC. For 6H-SiC the barrier height of Au-SiC was obtained to be 1.40±0.05V by Wu and Campbell[6]. In this section characteristics of Schottky barriers of undoped n-type 3C-SiC

fabricated with Au are mentioned.

Before vacuum evaporation of Au, samples were cleaned in organic solvent, acids, deionized water and a 20% hot solution of K_2CO_3. Cleaning in this hot solution was introduced by Suhara, and it was confirmed to be effective for the improvement of current voltage(I-V) characteristics of Schottky barriers[7].

Figure 9 shows an example of I-V characteristics of a Schottky diode fabricated with a grown layer on a (100) substrate. Figure 10 shows its log$I$-V plotting. Grown layers on 2° off substrates showed no meaningful differences in characteristics of Schottky barriers. The breakdown voltage of the fabricated diodes was at most about -5V and they showed "soft" breakdown. About the breakdown discussion is given afterwards.

In log$I$-V plotting an ideal factor n and a saturation current density J_0 are obtained. Using them I-V characteristics of a Schottky barrier is given as follows[8].

$$J=J_0(\exp(qV/nkT)-1) , \quad (3)$$

where J is current density, q elemental charge, V applied voltage, k Boltzmann constant and T absolute temperature. Though n should be 1.0 ideally, n is greater than 1.0 for real Schottky barriers. Using the value of J_0 the barrier height can be estimated[8]. However, J_0 showed wide variation in this investigation. Fundamentally the barrier height should be peculiar to the combination of a metal and a semiconductor and J_0 should not change. The values of n also showed wide variation. The smallest value of n was 1.27 and it was usually greater than 1.4. When the n value was close to the ideal value of 1.0, J_0 was relatively small. Therefore, some excess currents were considered to make J_0 larger. Since the introduction of guard rings showed no meaningful reduction of the current, surface leakage current was not a main factor of the excess currents. The barrier height estimated by capacitance-voltage characteristics also changed randomly. Photoelectric measurement[8] was attempted to estimate the barrier height. The obtained value for Au-SiC Schottky barriers by this method was 1.02eV. Yoshida et al.[9] reported a

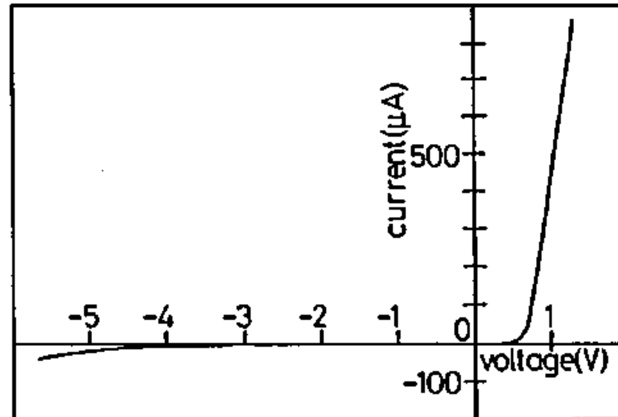

Fig.9 Current-voltage characteristics of a Au-3C-SiC Schottky diode.

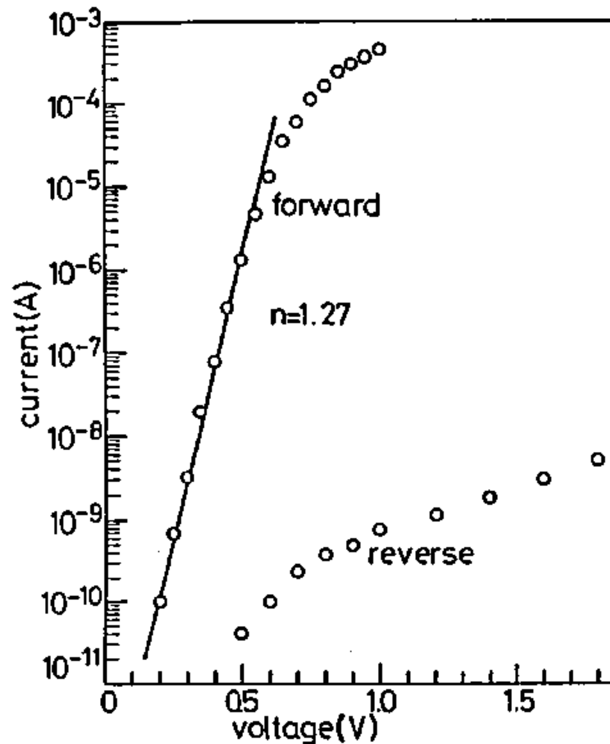

Fig.10 Log$I$-V plotting of current-voltage characteristics of a Au-3C-SiC Schottky diode.

value of 1.11eV by the same method. Schottky barriers were also fabricated using refractory metals such as Pt, Pd, Mo and W. The Schottky barriers with Pd showed comparable rectification to those fabricated with Au. Others were inferior in reproducibility. The barrier height of Pd-SiC measured by a photoelectric method was also 1.02eV.

No one reported about breakdown electric field in 3C-SiC up to now. Breakdown in Schottky diodes can be treated similar to a p^+n junction diode. Sze and Gibbsons[10] empirically achieved the following relationship between bandgap energy E_g and breakdown voltage V_b in one-sided p^+n and n^+p abrupt junctions.

$$V_B=60(E_g/1.1)^{3/2}(N_b/10^{16})^{-3/4} \quad (V) , \qquad (4)$$

where N_b is back ground impurity concentration. The maximum field E_m in a depletion layer is given as follows.

$$E_m= \left(\frac{2qN_b(V_B+V_d)}{\varepsilon_s}\right)^{1/2} \simeq \left(\frac{2qN_bV_B}{\varepsilon_s}\right)^{1/2} , \qquad (5)$$

where V_d is built-in potential and ε_s permittivity of a semiconductor. Since V_d is smaller than about 1V, it can be neglected for preliminary estimation. V_B and E_m were calculated as a function of N_b for 6H-SiC, 3C-SiC, GaAs, Si and Ge as shown in Figs.11(a) and (b). V_B and E_m obtained by Glover[11] using 6H-SiC Schottky diodes fabricated with Au were in accord with the Sze and Gibbsons's prediction. von Muench and Pfaffeneder[12] obtained higher E_m in one-sided p-n^+ junction diodes of 6H-SiC. In the case of 3C-SiC, V_B was calculated to be 30V for N_b of $1\times10^{17}cm^{-3}$ and 60V for $4\times10^{16}cm^{-3}$. A typical breakdown voltage of 4-5V was very small compared with these calculated values. There are many considerable origins of lowering the breakdown voltage such as tunneling[13], surface leakage, partial field enhancement, inappropriate surface treatment and crystal defects. Concerning these origins discussions are carried out one by one below. When the carrier concentration is very high and a depletion layer is very thin, tunneling takes place very easily. However, in the case of this investigation the carrier concentrations of most samples were lower than $1\times10^{17}cm^{-3}$, and this value is not so high as tunneling conduction occurs. Since

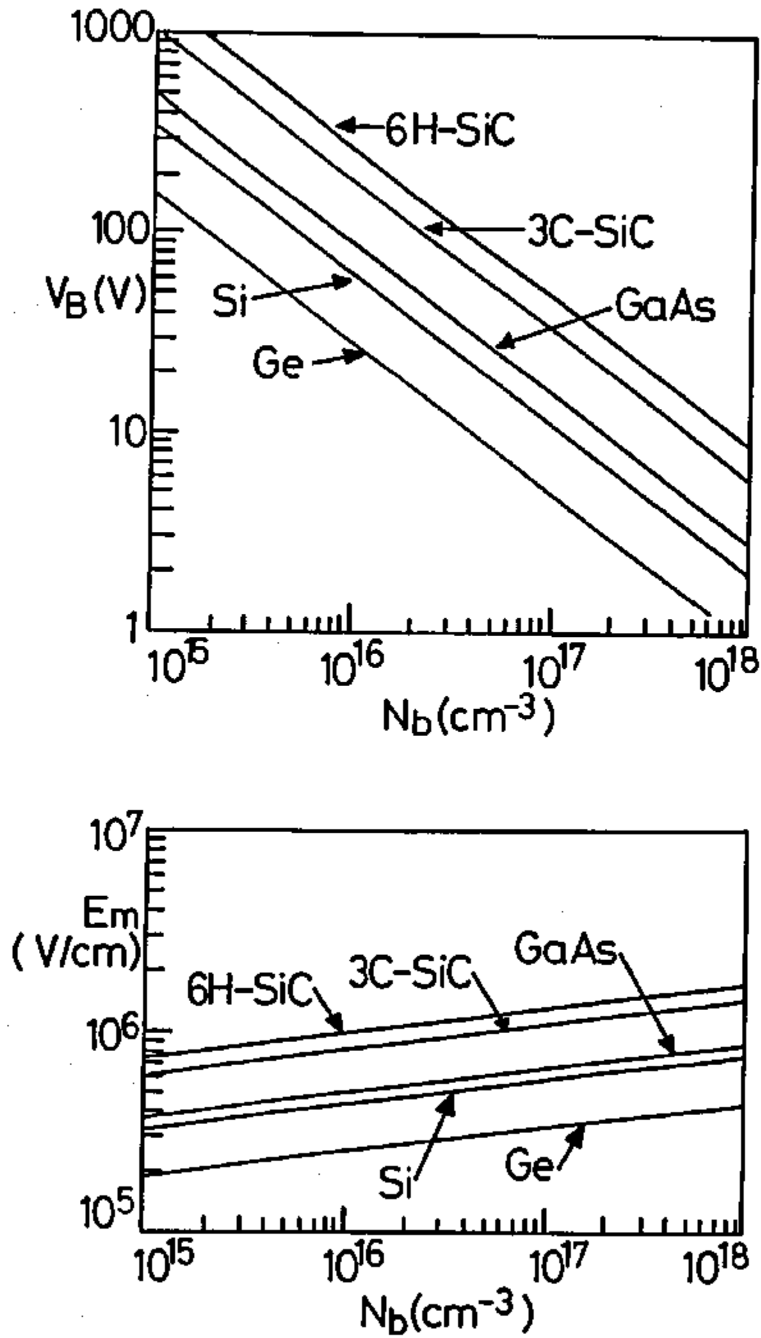

Fig.11 Predicted (a)breakdown voltage V_B and (b)maximum field E_m for onesided abrupt p-n junctions as a function of a background impurity concentration N_b. Used formulas were given by Sze and Gibbsons[10].

the reduction of the current due to the introduction of a guard electrode was very slight, surface leakage current was negligible. Surface roughness shown in the previous chapters can be an origin of partial field enhancement in Schottky barriers. However, there is no idea concerning how the breakdown voltage is really affected by the surface roughness. 3C-SiC is cleaned in a hot solution of K_2CO_3 before vacuum evaporation of Au in the current fabrication process. Suhara[7] reported that by the introduction of this cleaning an improvement of *I-V* characteristics in the forward biased region was observed as a reduction of the *n* value and saturated current density of J_0. And Suzuki[14] reported that samples without this cleaning sometimes showed very poor rectification. Thus, surface treatment seems very important for fabrication of Schottky barriers and some other cleaning or etching methods had better be attempted to improve their characteristics. As mentioned in Chapter II, 3C-SiC layers grown on Si substrates contains crystal defects, and the reduction of defect density due to the increase of the film thickness was observed. Schottky barrier diodes fabricated with grown layers with a thickness thinner than 1μm often showed very worse rectification. This result is considered to mean that characteristics of Schottky barriers are severely affected by defect density.

To sum up these discussion, there is no conclusive evidence for the low breakdown voltage, however, some following matters are probably effective to increase the breakdown voltage such as the improvement of surface flatness, a new surface treatment method and decrease of crystal defects.

3. B and Al doping

3-1 B-doping

Figures 12(a)-(c) show a variation of surface morphology due to the increase of a flow rate of B_2H_6 on (100) substrates. As

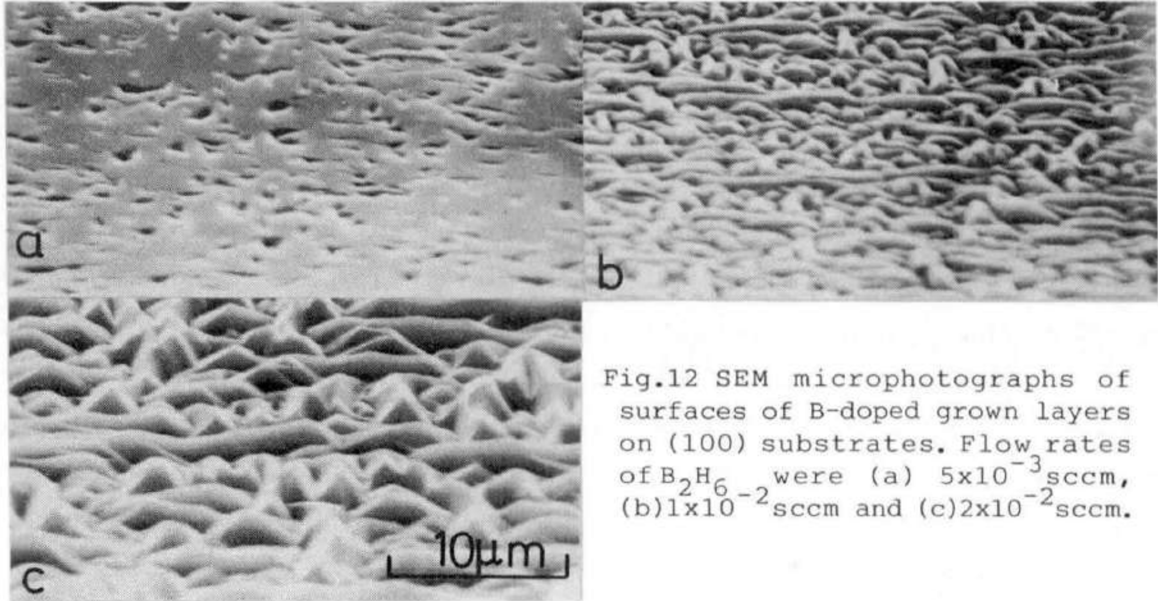

Fig.12 SEM microphotographs of surfaces of B-doped grown layers on (100) substrates. Flow rates of B_2H_6 were (a) $5x10^{-3}$sccm, (b)$1x10^{-2}$sccm and (c)$2x10^{-2}$sccm.

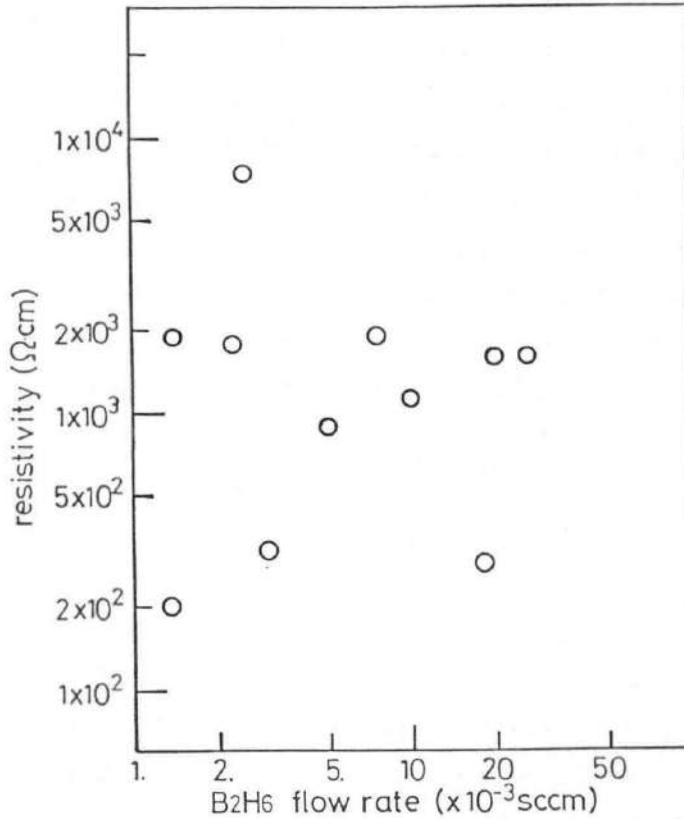

Fig.13 Resistivity of B-doped grown layers as a function of a flow rate of B_2H_6.

the flow rate increased surface roughness increased. When the flow rate of B_2H_6 was smaller than about $4x10^{-3}$sccm, flatness of the surface was comparable to that of the undoped layers. Figure 13 shows resistivities of the grown layers as a function of a B_2H_6 flow rate. When the flow rate of B_2H_6 was greater than about $1x10^{-3}$sccm, most of the grown layers showed resistivity higher than 200Ωcm. The highest resistivity was $8x10^3$Ωcm. By van der Pauw measurement of the grown layer for a flow rate of B_2H_6 of $4x10^{-3}$sccm, the resistivity, carrier concentration and hole mobility were obtained to be 320Ωcm, $1.1x10^{15}cm^{-3}$ and $18cm^2/Vs$, respectively. P-type conduction was confirmed at the same time. However, Al-Si electrodes which are usually used for p-type SiC mostly did not show good ohmic characteristics and Hall measurements by van der Pauw method was impossible and the values of the carrier concentration and hole mobility were not clear.

Thus by B-doping high resistive p-layers were obtained. If the high resistivity of the B-doped layer is maintained even at high temperatures, it is useful for device applications. However, rapid reduction of the resistivity was observed by heating as shown in Fig.14. The rapid reduction of the resistivity was due to a rapid increase of the carrier concentration. The carrier concentration was $8.6x10^{14}cm^{-3}$ at 25°C and it increased to $5.8x10^{16}cm^{-3}$ at 130°C as shown in Fig.15. Such a rapid change of electrical characteristics is due to a large activation energy of a B acceptor. Using the measured temperature dependence of the carrier concentration in Fig.15, the activation energy was estimated to be 413meV. This value is smaller than that of 735meV obtained by photoluminescence measurements[15]. Though further investigation is necessary to obtain an exact activation energy, there is no doubt that its value is extraordinary large.

3-2. Al-doping

For Al doping TEA and TMA were used. Figure 16 shows the relationship between their vapor pressure and temperatures. Since TEA has low vapor pressure at room temperature a vessel of TEA

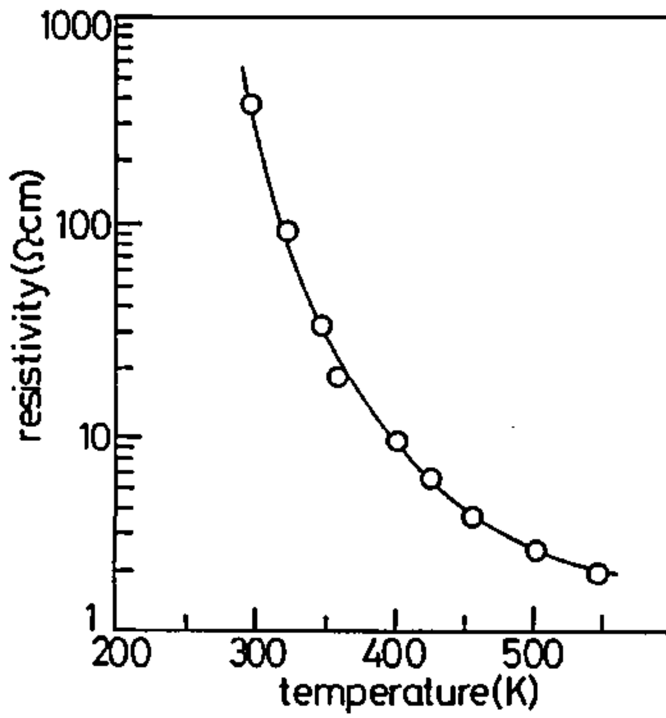

Fig.14 Temperature dependence of resistivity of a B-doped grown layer.

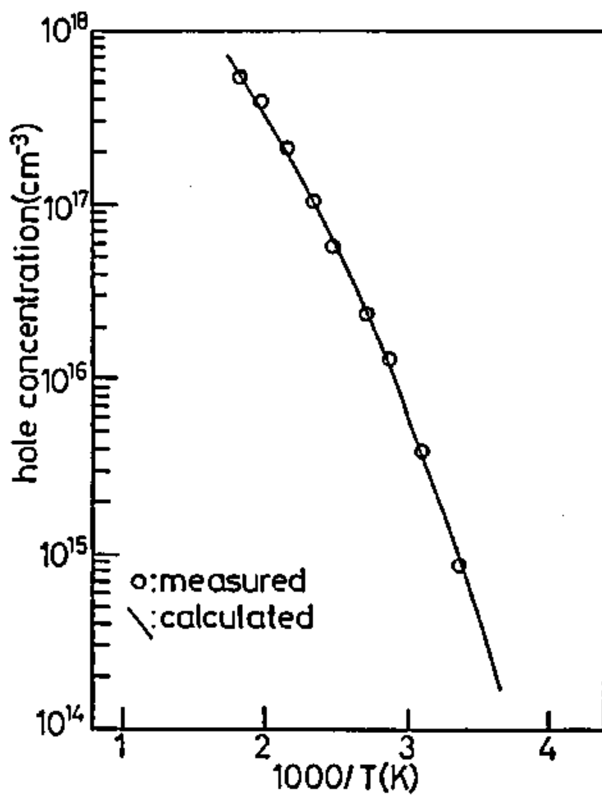

Fig.15 Temperature dependence of hole concentration of a B-doped grown layer.

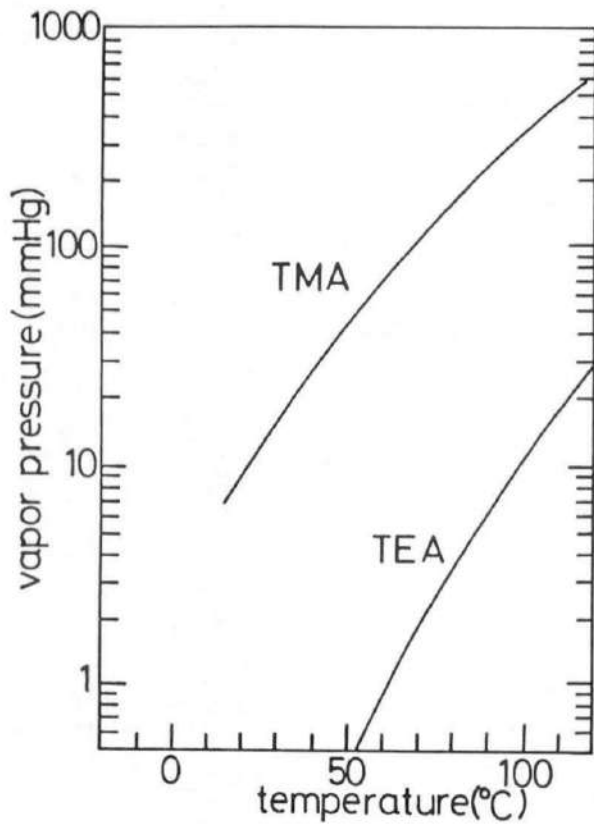

Fig.16 Vapor pressures of TMA and TEA as a function of temperature.

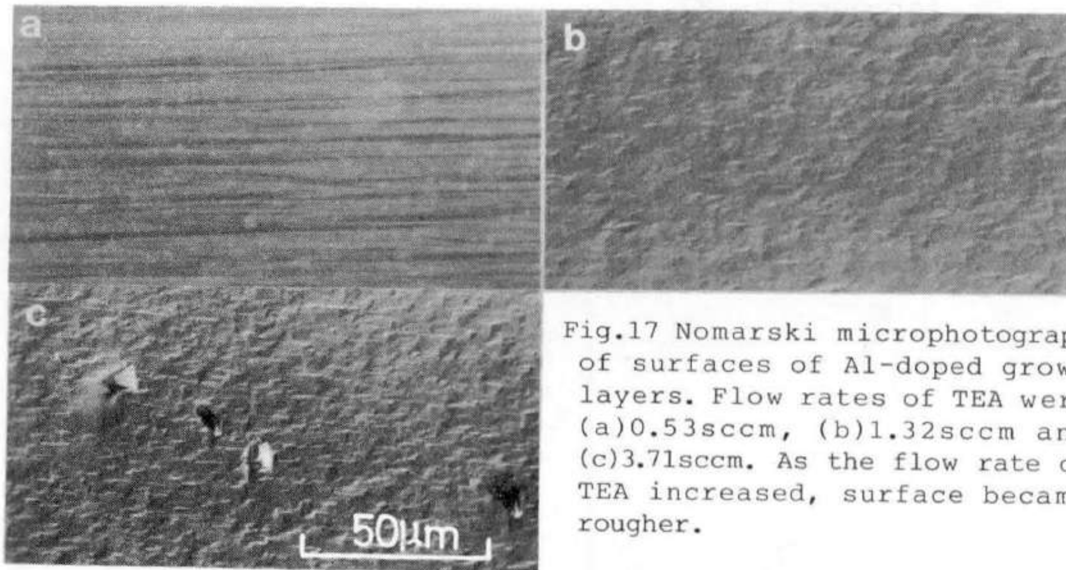

Fig.17 Nomarski microphotograph of surfaces of Al-doped grown layers. Flow rates of TEA were (a)0.53sccm, (b)1.32sccm and (c)3.71sccm. As the flow rate of TEA increased, surface became rougher.

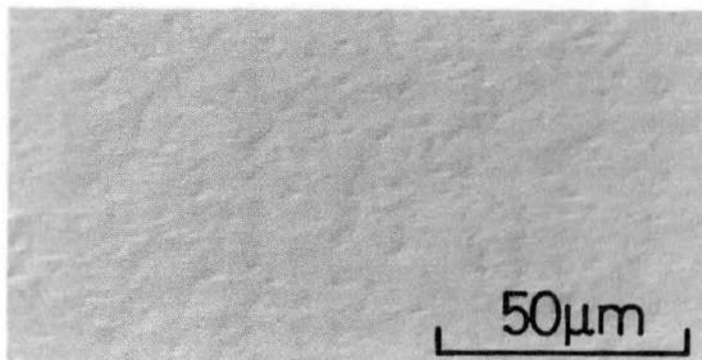

Fig.18 By the reduction of C_3H_8 flow rate during Al-doping, surface flatness was improved. Flow rate of TEA was 1.95sccm. The flow rate of C_3H_8 was reduced from 0.32 to 0.15sccm.

was heated in the range of 62-120°C. The flow rate of TEA was controlled by changing both the temperature of the vessel and the flow rate of bubbling H_2. To avoid liquefaction on the way to a reaction tube, stainless tubes between the vessels and the reaction tube were also heated. However, liquefaction was not prevented perfectly. To keep controlability of the TEA flow rate long-time evacuation was sometimes necessary. The maximum flow rate of H_2 for bubbling was 100sccm in this investigation. The combination of the low vessel temperature and the higher flow rate of bubbling H_2 is probably preferable to prevent such a problem. If bubbling is carried out by a carrier gas, the temperature of the vessel is able to be kept below 60°C. Since TMA has large enough vapor pressure at room temperature, the temperature of the vessel was maintained at 20°C and the flow rate of TMA was controlled by changing the flow rate of bubbling H_2.

Figures 17(a)-(c) show a variation of surface morphology of Al-doped layers on 2° off substrates due to the change of the TEA flow rate. Grown layers doped with TMA showed similar results. When the flow rate of TEA was 0.53sccm the surface morphology was comparable to undoped layers. As the flow rate of TEA increased, surface roughness increased and needle-like growth appeared as shown in Figs.17(b) and (c). The observed variation of the surface morphology due to doping with organic Al was similar to the variation caused by the increase of a carbon source. In the case of the sample of Fig.17(b) the flow rates of C_3H_8 and TEA were 0.32sccm and 1.95sccm, respectively. The amount of introduced carbon atoms by TEA was about 18 times larger than that by C_3H_8. TEA was considered to work as a carbon source. The flow rate of C_3H_8 was reduced to 0.15sccm. The surface flatness recovered and needle-like growth disappeared as shown in Fig.18. This variation of the surface morphology supports that TEA works as a carbon source. Further reduction of the C_3H_8 flow rate resulted in rough surfaces again. Figure 19 shows an example of the relationships between electrical properties and the flow rate of organic Al. Electrical properties were evaluated by van der

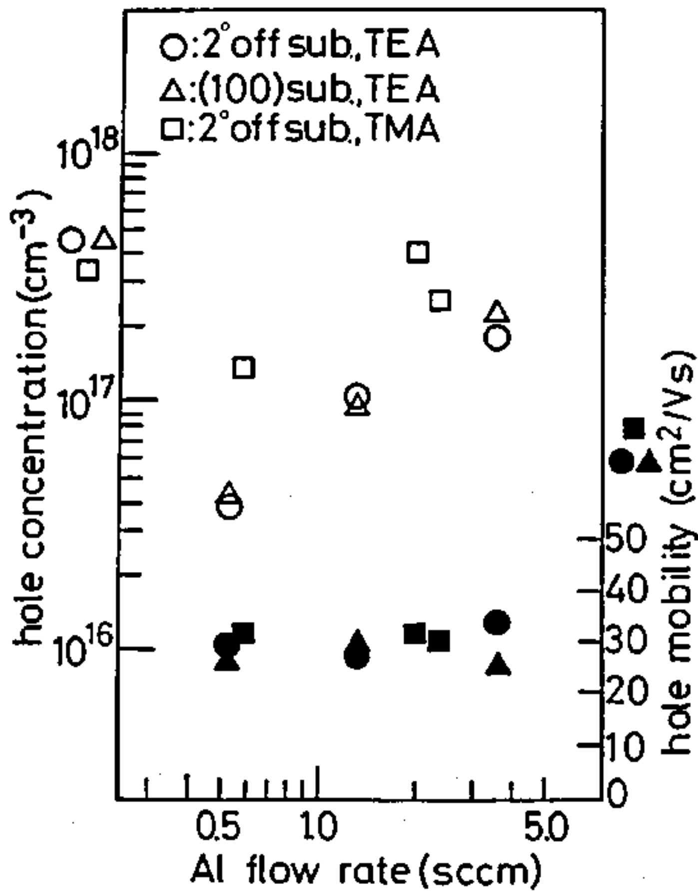

Fig.19 Hole concentration and mobility as a function of a flow rate of organic aluminum.

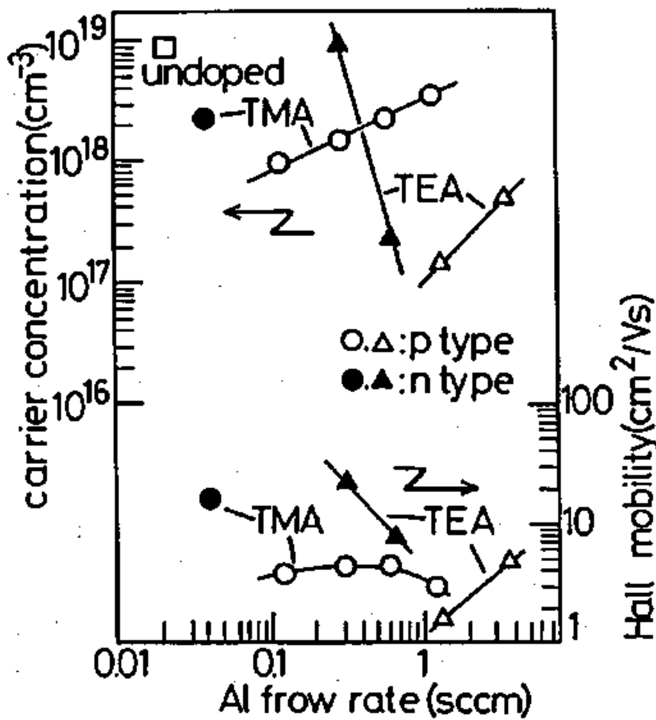

Fig.20 Carrier concentration and mobility as a function of flow rate of organic aluminum. The samples were grown under the condition of unusually high undoped carrier concentration. See text.

Pauw measurement. The grown layers were three types; i.e. grown layers on (100) and 2° off substrates doped with TEA and on 2° off substrates doped with TMA. P-type conduction was confirmed. The obtained hole concentrations were $4x10^{16}$-$6x10^{17}cm^{-3}$. The hole mobility was about $30cm^2/Vs$. When the undoped carrier concentration was very high($n \geq 10^{19}cm^{-3}$), the obtained hole concentration was also high as shown in Fig.20. The highest hole concentration of $4x10^{18}cm^{-3}$ was obtained at a TMA flow rate of 1.2sccm.

TEA-doped grown layers on (100) and 2° off substrates showed no meaningful differences in electrical properties as shown in Fig.19 different from undoped layers. The undoped layers on off substrates outwardly showed low electron mobility and low carrier concentration by van der Pauw measurement because of anisotropy. To clarify whether this result of Al-doped layers is due to the absence of anisotropy or not, Hall measurements as mentioned in Section 2-1 should be attempted. The R value which is nearly 1 for square and isotropic samples could not be utilized in this case. Because Al-doped layers were fragile and square samples were very difficult to prepare.

P-n junction diodes were fabricated. On n-type 2° off substrates, undoped and Al-doped layers were grown successively. Details of growth conditions are listed in Table 1. Mesa structures were formed using an Al mask by RIE(reactive ion etching) of CF_4 and O_2[16]. An example of I-V characteristics is shown in Fig.21. Rectification was not good. To improve characteristics an optimization of growth conditions and fabrication processes is probably necessary.

As mentioned before, organic Al simultaneously works as a dopant and a carbon source. Though the influence of organic Al could be reduced by decreasing the flow rate of C_3H_8, to improve controlability other Al-sources which contain less carbon are desirable. Nishino et al. used $AlCl_3$ as an Al source for CVD growth of 6H-SiC[15]. However, the flow rate control of $AlCl_3$ was difficult, because it is solid at room temperature and heating at temperatures above 200°C was necessary to obtain large enough

sub.: Si(100) 2° off
1st layer: undoped 6.6μm
2nd layer: TMA 0.04sccm, 1.6μm
3rd layer: TMA 0.36sccm, 0.2μm

SiH_4: 0.3sccm, C_3H_8: 0.27sccm

Table 1 Growth conditions of a p-n junction.

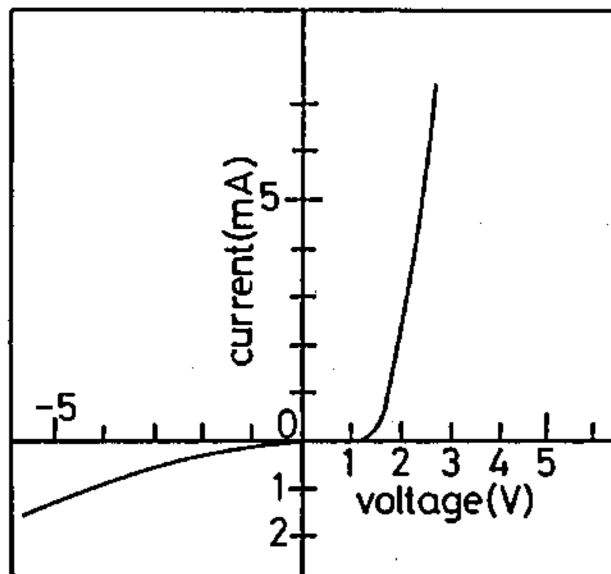

Fig.21 Current-voltage characteristics of a fabricated p-n junction diode.

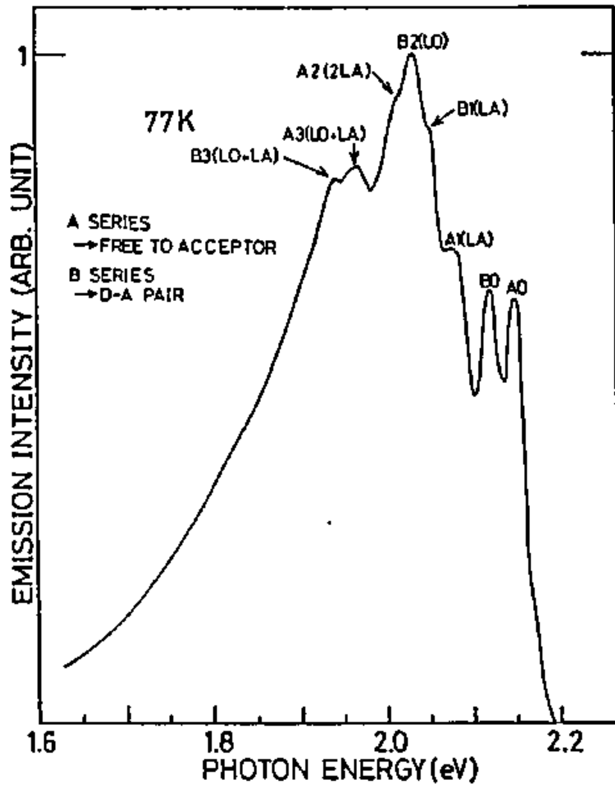

Fig.22 Typical photoluminescence spectrum of Al-doped grown layers.

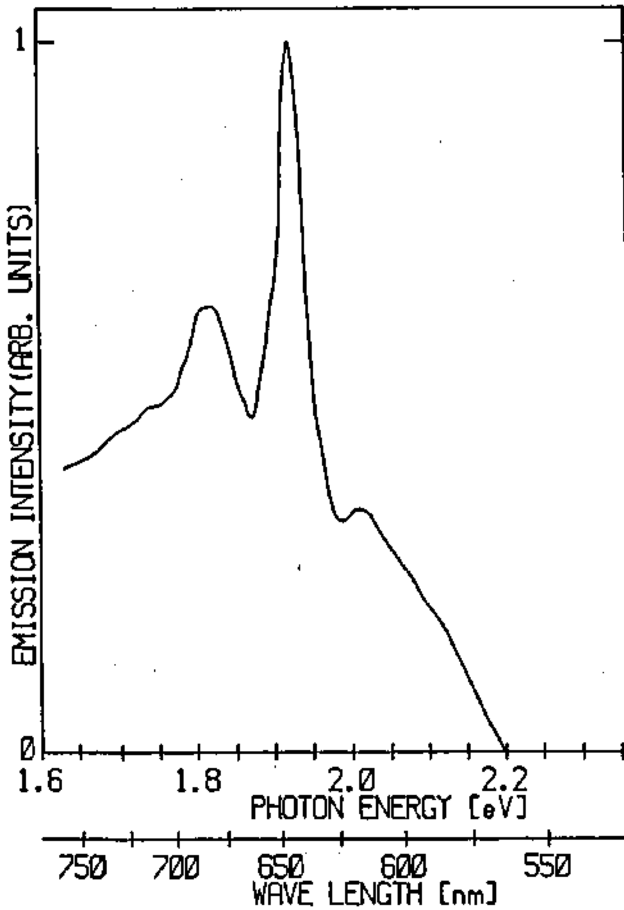

Fig.23 Photoluminescence spectrum of a undoped grown layer. Na was detected by SIMS analysis of this sample.

vapor pressure by sublimation. Moreover, $AlCl_3$ is deliquescence. Its merit is stability. Organic Al reacts with water and oxygen in flames and it is toxic. By considering these factors, $(CH_3)AlCl_2$ is interesting as a candidate of a dopant which takes the places of TEA and TMA. $(CH_3)AlCl_2$ is a white solid at room temperature and the melting and boiling points are 73°C and 152°C, respectively. The vapor pressure at 100°C is 100mmHg. This value is comparable to that of TMA at about 70°C. Its reactivity with water and oxygen is lower than TMA and TEA. Thus, it satisfies conditions necessary for new chemicals which take the places of TEA and TMA. An investigation of Al doping using $(CH_3)AlCl_2$ is expected.

4. Photoluminescence

SiC has an indirect band structure. In photoluminescence observation, light emission related to acceptors is mainly observed. In other words, to observe photoluminescence acceptor doping is sometimes necessary. In this work, Al-doping was carried out using TMA and TEA. Figure 22 shows an example of a photoluminescence spectrum of the Al-doped grown layer. A similar spectrum to Al-doped crystals prepared by a solution growth method[2] was obtained. Many peaks originated from two types of mechanisms were observed. A peak which has the highest energy and that at the second highest energy are due to free-to-bound acceptor recombination and donor-acceptor(N and Al) pair recombination, respectively. Their phonon-replicas were observed in the lower energy side. The intensity of the photoluminescence dropped as the the flow rate of organic Al increased. Doped Al or excessively supplied carbon by organic Al were considered to give rise to the drop in the intensity. There are three probable mechanisms of the drop in the intensity such as deterioration of crystallinity, generation of deep levels and change in recombination process.

Some undoped layers showed orange or red luminescence. Two

types of spectra were observed. Al was detected by the SIMS analysis of the samples which showed similar spectra to Fig.22. Some other samples showed similar spectra to Fig.23. Na was detected by the SIMS analysis for such a sample. A susceptor is one of the most likely candidates for a source of such metal impurities.

5. Summary

All undoped layers showed n-type conduction in Hall measurements. The highest electron mobility for the grown layers containing APD's on (100) substrates was $488cm^2/Vs$ with a carrier concentration of $3.18x10^{16}cm^{-3}$. Undoped carrier concentrations were usually in the range of $3x10^{16}$-$2x10^{17}cm^{-3}$. The grown layers on off substrates showed electrical anisotropy. $\mu_{\parallel}$ was about $500cm^2/Vs$ independent of off angle. $\mu_{\perp}$ decreased as the off angle became larger. Breakdown voltages of Au-SiC Schottky barriers were low compared with theoretically predicted values, and the breakdown was "soft". Improperness of surface treatment, surface roughness and crystal defects are probable origins of such breakdown problems.

To obtain p-layers B and Al were doped using B_2H_6 and organic Al, respectively. B-doped layers showed high resistive p-type conduction at room temperature. Organic Al worked simultaneously as both a dopant and a carbon source. The hole concentration was controlled in the range of $4x10^{16}$-$6x10^{17}cm^{-3}$ by changing a flow rate of organic Al. A typical hole mobility in Al-doped layers was about $30cm^2/Vs$.

References

[1] H.Kuwabara and S.Yamada, Phys. Status Solidi a 30(1975) 739.
[2] A.Suzuki, H.Matsunami and T.Tanaka, J. Electrochem. Soc. 124(1977) 241.

[3] H.Kuwabara, K.Yamanaka and S.Yamada, Phys. Status Solidi a 37(1976) K157.
[4] N.Mikoshiba, *Handoutai no Butsuri(Physics of Semiconductors)*, (Baifuukan, Tokyo, 1982), p.103, in Japanese.
[5] A.Suzuki, A.Uemoto, K.Furukawa, Y.Fujii, M.Shigeta and S.Nakajima, 48th Autumn Meeting of the Japan Society of Applied Physics, Nagoya, October, 1987, 17p-ZG-14.
[6] S.Y.Wu and R.B.Campbell, Solid State Electron. 17(1974) 683.
[7] H.Suhara, Master Thesis, Faculty of Engineering, Kyoto University, 1983.
[8] S.M.Sze, *Physics of Semiconductor Devices*, (Wiley, New York, 1981) 2nd ed., Chapter 5.
[9] S.M.Sze and G.Gibbsons, Appl. Phys. lett. 8(1966) 111.
[10] S.Yoshida, K.Sasaki, E.Sakuma, S.Misawa and S.Gonda, Appl. Phys. Lett. 46(1985) 766.
[11] G.H.Glover, J. Appl. phys. 46(1975) 4842.
[12] W. von Muench and I.Pfaffeneder, J. Appl. Phys. 48(1977) 4831.
[13] A.G.Chynoweth, W.L.Feldmann, C.A.Lee, R.A.Logan, G.L.Pearson and P.Aigrain, Phys. Rev. 118(1960) 425.
[14] A.Suzuki, private communication(1986).
[15] S.Nishino, A.Ibaraki, H.Matsunami and T.Tanaka, Jpn. J. Appl. Phys. 19(1980) L353.
[16] S.Dohmae, K.Shibahara, S.Nishino and H.Matsunami, Jpn. J. Appl. Phys. 24(1985) L873.

V. ION IMPLANTATION INTO 3C-SiC GROWN LAYERS AND APPLICATION TO MOSFET'S

1. Introduction

A selective doping technique is indispensable in fabrication of electronic devices especially for IC(integrated circuits). There are two major techniques for selective doping, namely, diffusion and ion implantation methods. Both methods are popular for a Si process. However, in the case of SiC the diffusion method is hard to apply, because the diffusion coefficients of impurities in SiC are very low. Campbel and Chang fabricated junction-gate FET's of α-SiC using a diffusion technique[1]. They reported that diffusion of Al into α-SiC required temperatures from 1800°C to 2100°C. Moreover, a special masking technique utilizing SiC was necessary. Thus, the diffusion method seems to be not practical for SiC. Ion implantation into α-SiC was attempted by many investigators[2-6]. Marsh investigated the activation of implanted impurities using various dopants[2]. Though the implantation of donor impurities such as N, P, Sb and Bi was successful, samples implanted with acceptors were high resistive even after annealing and the acceptors could not be activated. They explained that deep donor-type defects induced by the implantation prevented the activation of the implanted acceptors. Concerning 3C-SiC Kalinina et al.[7] reported a successful fabrication of p-n junction diodes by implantation of Al, however, they did not describe details of investigation. Though Kondo et al.[8] attempted hot implantation(specimens were intentionally heated during implantation) in addition to the standard implantation, the activation was unsuccessful. Edmond et al.[9] reported successful fabrication of p-n junction diodes by hot implantation of Al into undoped layers without annealing. The crystal growth methods of these two groups are similar to that of this investigation. The difference in their investigations is not clear.

In this investigation, implantation of N_2^+ and P^+ was attempted. The electrical characteristics of implanted layers were evaluated changing annealing temperatures. Planar-type p-n junction diodes were fabricated using the implantation technique.

The first successful fabrication of n-channel inversion-type MOSFET's is mentioned. The MOSFET's were fabricated by the combination of ion implantation and thermal oxidation techniques which are ordinary in the Si process.

2. Activation of implanted donors

Ion implantation of N_2^+ and P^+ was carried out into B-doped grown layers. High resistive($\rho \geq 200\Omega cm$) B-doped layers were suitable for characterization of thin n^+ layers formed by implantation of donors. The thickness of the B-doped grown layers was about 6μm. APD-free grown layers on 2° off substrates were used. Samples were tilted at 7° during the implantation to avoid a channeling effect. The current density of an ion beam was lower than $0.25\mu A/cm^2$. Therefore, heating by the beam during the implantation was negligible[10].

The conditions of the ion implantation were listed in Table 1. The implantation was carried out by successive two steps to improve the uniformity of implanted impurities. The first implantation was high dose with high energy and the second was low dose with low energy. Figure 1 shows a calculated profile of implanted P using the projected average range and projected standard deviation in the literatures[11-13] for a total dose of $1.3x10^{15}cm^{-2}$(condition 1 in Table 1). In the case of condition 2, the total dose was decreased to 30% of that in condition 1 with the same energy. N_2^+ implantation with a total dose of $1.95x10^{14}cm^{-2}$(condition 3) corresponds to N^+ implantation with a dose of $3.9x10^{14}cm^{-2}$ which is the same dose level as condition 2. The energy of the N_2^+ implantation was decided to have the nearly same impurity profile[13] as in P^+ implantation of condition 2. After the implantation samples were annealed in

No.	implanted ion	1st dose(cm^{-2}) 2nd	1st energy(eV) 2nd	total dose (cm^{-2})
1	P^+	$1x10^{15}$ $3x10^{14}$	100K 25K	$1.3x10^{15}$
2	P^+	$3x10^{14}$ $9x10^{13}$	100K 25K	$3.9x10^{14}$
3	N_2^+	$1.5x10^{14}$ $4.5x10^{13}$	100K 25K	$1.95x10^{14}$

Table 1 Conditions of ion implantation.

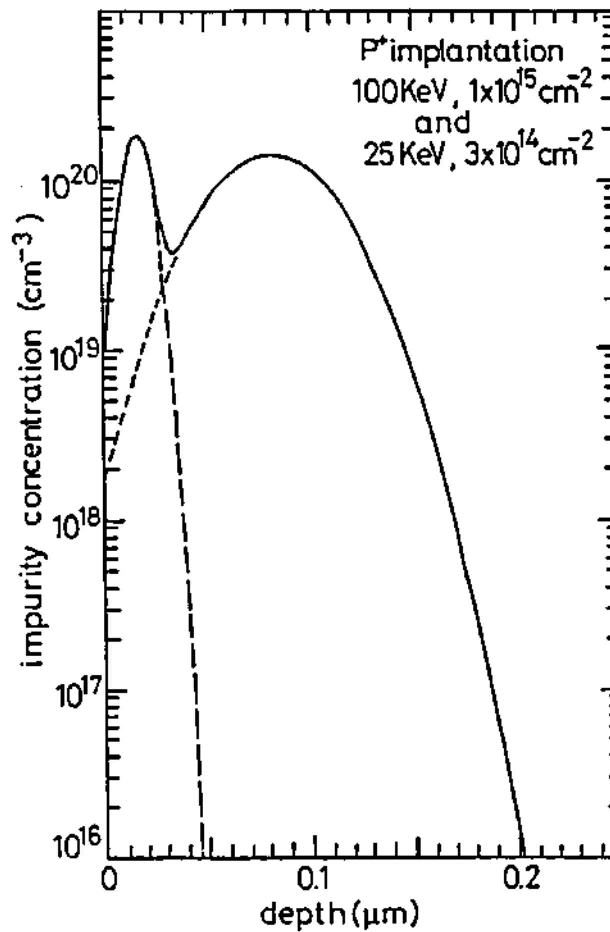

Fig.1 Calculated profile of implanted P with a total dose of $1.3x10^{15}cm^{-2}$. Details of conditions of implantaion are listed in Table 1.

Ar atmosphere for 30min. The samples were heated by RF inductive heating. By SIMS analysis the annealed specimen showed almost the same depth profile of implanted P as that without annealing by SIMS analysis.

Figure 2(a) shows a RHEED halo pattern of an as-implanted sample. The ion implantation was carried out under condition 1(P^+, total dose: $1.3x10^{15}cm^{-2}$). The halo pattern indicates that the implanted layer was amorphous. Figure 2(b) shows a RHEED pattern of the sample after annealing at 800°C. Recrystallization to a single crystal was clearly observed. Annealing temperature was changed up to 1300°C. However, no significant difference in RHEED patterns compared with Fig.2(b) was observed. Samples implanted under condition 2(P^+, total dose: $3.9x10^{14}cm^{-2}$) showed similar results. The implanted samples could be told from not implanted samples with naked eyes by noticing a slight difference in colors. The refractive index of the implanted layers changed by amorphization and interference took place. The difference in colors vanished by annealing.

Sheet resistance of the implanted layers was evaluated by the four-point probe method or by van der Pauw method. Si substrates of the specimens for van der Pauw measurement were removed by a mixed solution of HNO_3 and HF before the measurement to avoid errors due to current conduction through the substrates. N-type conduction was confirmed for both the P^+ and N_2^+ implanted layers by van der Pauw method. As shown in Fig.3, the sheet resistance monotonously decreased as annealing temperature increased and it reached to about $10^3\Omega/\square$by annealing at about 1350°C.

Electrical activation rates were estimated by van der Pauw measurement. The electrical activation rate was defined as the ratio of sheet carrier concentration and total dose. The electrical activation rates were improved by raising annealing temperatures as shown in Fig.4. The P^+ implanted layer with a total dose of $3.9x10^{14}cm^{-2}$(condition 2) gave the higher electrical activation rates than those for a total dose of $1.3x10^{15}cm^{-2}$(condition 1). The N_2^+ implanted layers gave the

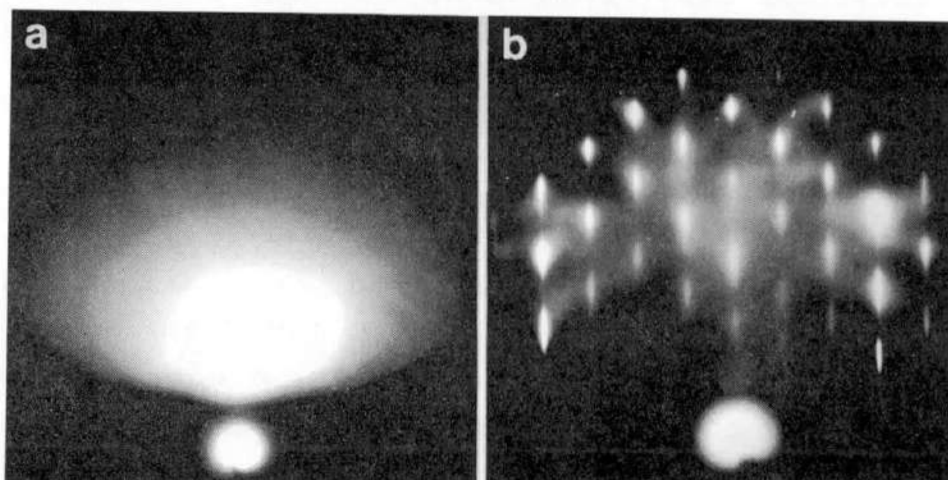

Fig.2 RHEED patterns of P^+ implanted layers. (a)Before and (b)after annealing at 800°C.

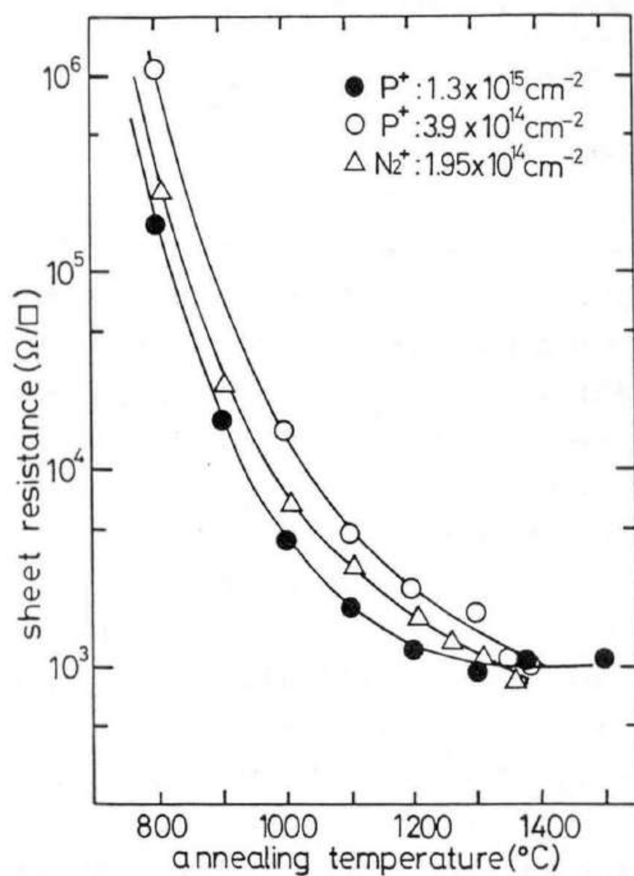

Fig.3 Sheet resistance of implanted layers as a function of annealing temperatures.

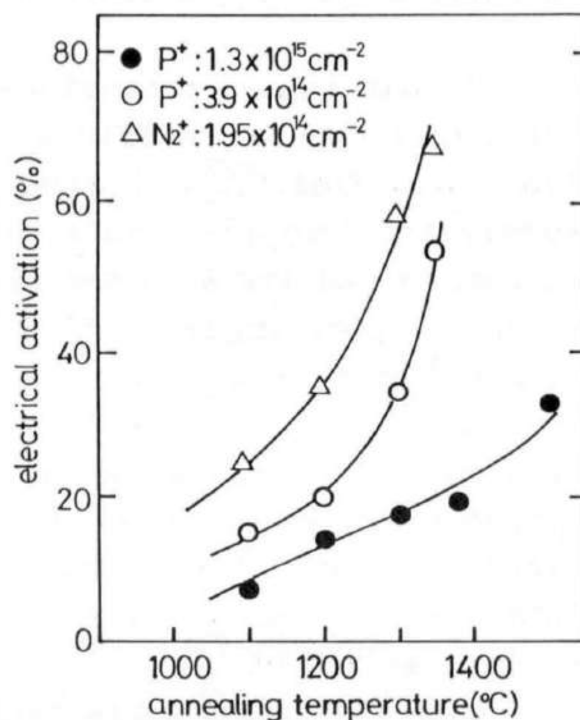

Fig.4 Electrical activation rate as a function of annealing temperatures.

higher electrical activation rates than the P^+ implanted layers, which is similar to implantation into 6H-SiC[2]. Bridge-type specimens were fabricated by the P^+ implantation to carry out the standard Hall measurement and to investigate electrical anisotropy in the implanted layers. Such specimens were fabricated by a selective implantation utilizing a deposited SiO_2 film as a mask. The implantation was carried out under condition 2. Concerning conditions 1 and 3 the standard Hall measurement was not carried out yet. The electrical activation rates obtained by the standard Hall measurement well agreed with those obtained by van der Pauw measurement. The electron mobility obtained by van der Pauw method was about $30cm^2/Vs$ in all cases. The electron mobility obtained by the standard Hall measurement showed electrical anisotropy similar to the undoped grown layers. $\mu_{\parallel}$ and $\mu_{\perp}$ were about 50 and $25cm^2/Vs$, respectively.

3. Fabrication of p-n junction diode

Planar-type p-n junction diodes were fabricated using the ion implantation technique. Figure 5 shows the structure of fabricated diodes. An Al-doped p-layer was grown on a 2° off p-Si substrate. Typical hole concentration, hole mobility and resistivity of the Al-doped layer were $3.5x10^{17}cm^{-3}$, $32cm^2/Vs$ and $0.56\Omega cm$, respectively. P^+ implantation with a total dose of $3.9x10^{14}cm^{-2}$ or N_2^+ with a total dose of $1.95x10^{14}cm^{-2}$ was carried out to obtain n-layers. Deposited SiO_2 of 500nm in thickness was used as a mask for the implantation. Annealing temperatures were 1100°C, 1200°C and 1300°C. Annealing time was fixed at 30 min. Finally ohmic contacts were formed using Al and AuGa for n-SiC and p-Si, respectively. The area of the fabricated diodes was $7.1x10^{-4}cm^2$.

Current-voltage characteristics of the P^+ and N_2^+ implanted diodes were shown in Figs.6(a) and (b), respectively. Both the P^+ and N_2^+ implanted diodes showed similar results. Rectification of the diodes annealed at 1100°C and 1200°C was superior to those

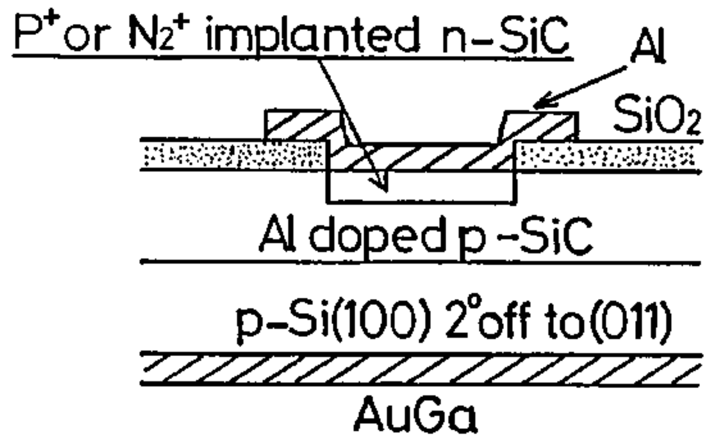

Fig.5 Schematic cross section of planar type p-n junction diodes fabricated by the ion implantation.

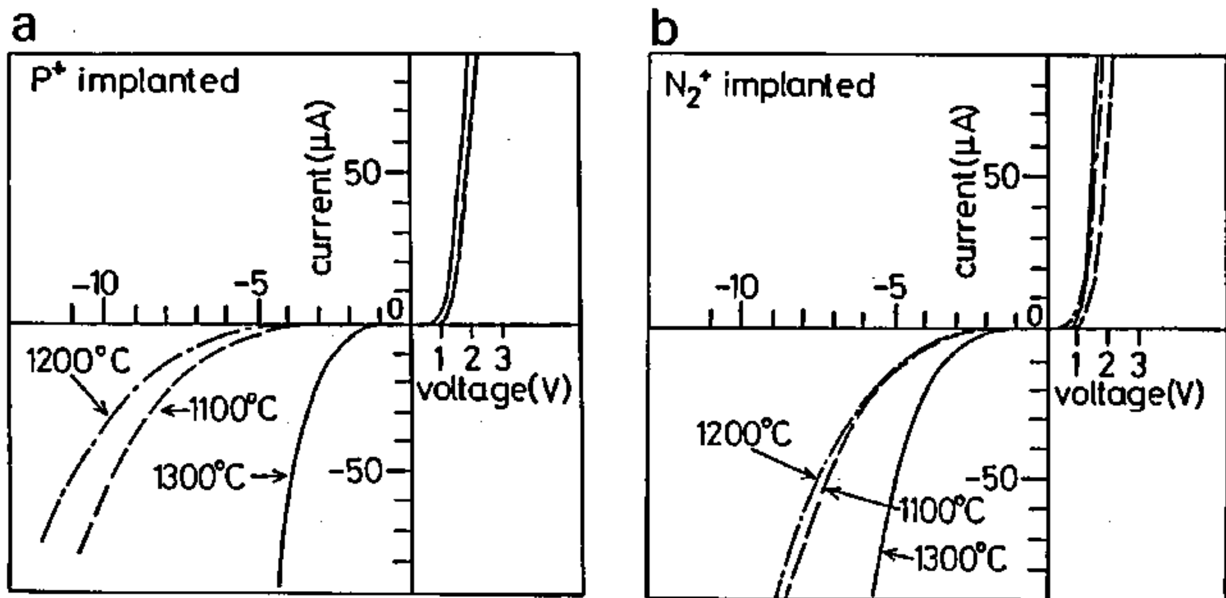

Fig.6 Current-voltage characteristics of p-n junction diodes fabricated by (a)P^+ and (b)N_2^+ implantation.

at 1300°C. As shown in Fig.4, the electrical activation rate increased abruptly by annealing at temperatures over 1300°C. And so, this annealing temperature dependence of the rectification was considered to be related to the change from an n-layer to an n^+-layer because of increase in the electrical activation rate. The best ideal diode factor of 3.8 was obtained when annealing temperature was 1100°C for both the P^+ and N_2^+ implanted diodes.

Capacitance-voltage characteristics of these diodes showed small variation in capacitance as shown in Fig.7. As annealing temperatures were raised, the capacitance and the magnitude of its variation became larger. These results mean that the diodes had p-i-n structures[14] and the thickness of the i layer became thinner as annealing temperature became higher. The N_2^+ implanted diodes showed the larger capacitance and its variation than the P^+ implanted diodes. This difference was considered to originate from the difference in electrical activation. The N_2^+ implanted layers showed the higher electrical activation rates than the P^+ implanted layers as mentioned in the previous section. Hence, the thicknesses of the i layers were thinner in the N_2^+ implanted diodes and the capacitance became larger.

4. Fabrication of MOSFET's

MOSFET's were fabricated using the ion implantation technique. A schematic cross section of the fabricated MOSFET's is shown in Fig.8. A channel layer of B-doped p-SiC with the thickness of 2μm was grown on undoped n-SiC with the thickness of 7μm. Since there is large lattice mismatch between Si and SiC, the layer with the thickness of over several microns was necessary to reduce crystal defects and to improve device characteristics by our present technique. Source and drain were formed by the ion implantation of P^+ using deposited SiO_2 with the thickness of 500nm as a mask. The implantation was carried out under the condition 1 in Table 1. Annealing after the implantation was carried out in an IR radiative heating furnace

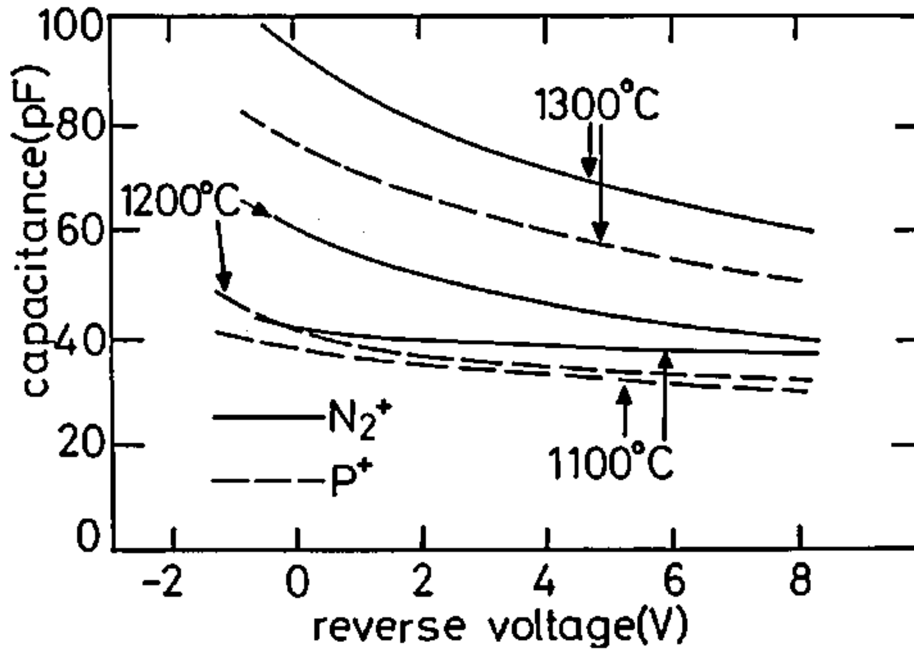

Fig.7 Capacitance-voltage characteristics of p-n junction diodes.

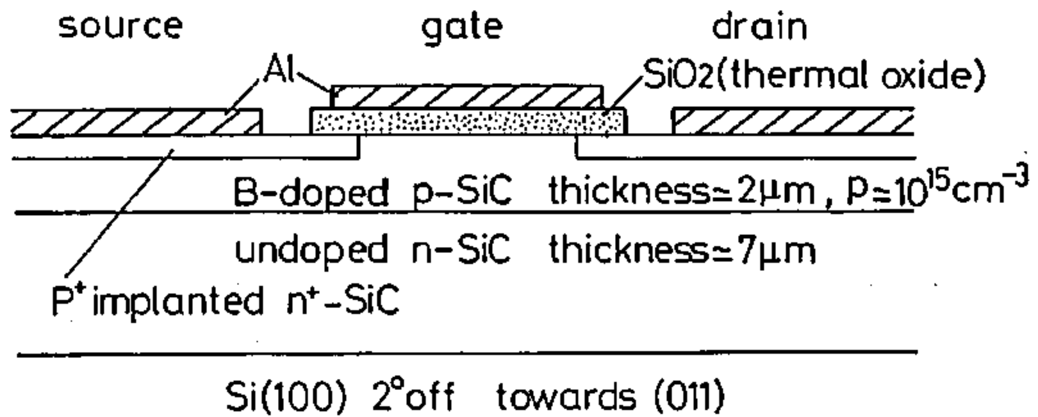

Fig.8 Schematic cross section of fabricated MOSFET's.

in Ar atmosphere at 1080°C for 1hr.

A gate insulator was formed by thermal oxidation of SiC at 1050°C using dry oxygen for 6hrs. The thermal oxide film of 3C-SiC was found to be SiO_2 and inversion was confirmed under an illuminated condition in an Al/SiO_2/n-SiC structure[15]. Typical electrical resistivity and breakdown electric field of SiO_2 formed by the thermal oxidation were $8.5\times10^{15}\Omega$cm and 2.5×10^{6}V/cm, respectively. The thickness of the gate oxide was about 60nm. The gate length and the width are 20μm and 500μm, respectively. Al was used as a gate electrode and ohmic contacts for source and drain. Alloying of the ohmic contacts was not carried out. The top view of the fabricated MOSFET is shown in Fig.9.

Current-voltage characteristics of the FET at 310K are shown in Fig.10. The sample was not illuminated. An action of inversion-type MOSFET's was achieved for the first time. Kinks in the saturation region were observed. Such kinks are known as a feature of SOI(Si-on-insulator) MOSFET's[16,17]. Since in this investigation the MOSFET's were fabricated on a high resistive B-doped p-layer, their characteristics were considered to show SOI-like features. In Al-SiO_2-SiC MOS diodes, the inversion condition was observed only under illumination, which is due to very low intrinsic carrier concentration($\simeq 10$cm^{-3} at 300K) of 3C-SiC[15]. However, the MOSFET's operated without illumination. Electrons which are necessary to form an inversion layer were considered to be supplied from source.

Effective mobility of the FET was estimated using the characteristics in the linear region where drain voltage was lower than the voltage at the beginning of the kink. Ideal characteristics of MOSFET's in the linear region are given by

$$I_d=(W/L)\mu_n C_0((V_g-V_{th})V_d-V_d^2/2) \quad , \qquad (1)$$

where I_d is drain current, W gate width, L gate length, μ_n electron mobility, V_g gate voltage, V_{th} threshold voltage and V_d drain voltage. Here W/L is 25 and the value of 5.75×10^{-8}F/cm^2 was used for C_0 based on an investigation of Al-SiO_2-SiC system[15]. μ_n and (V_g-V_{th}) were changed to agree with measured I_d-V_d

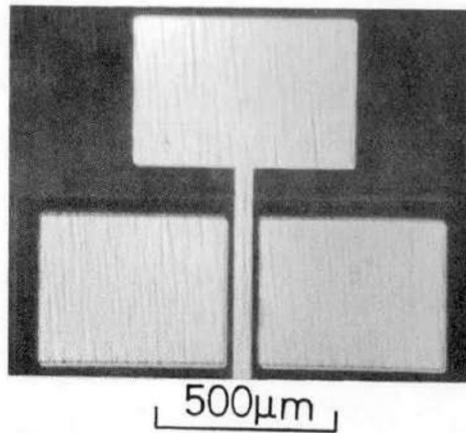

Fig. 9 Top view of a fabricated MOSFET.

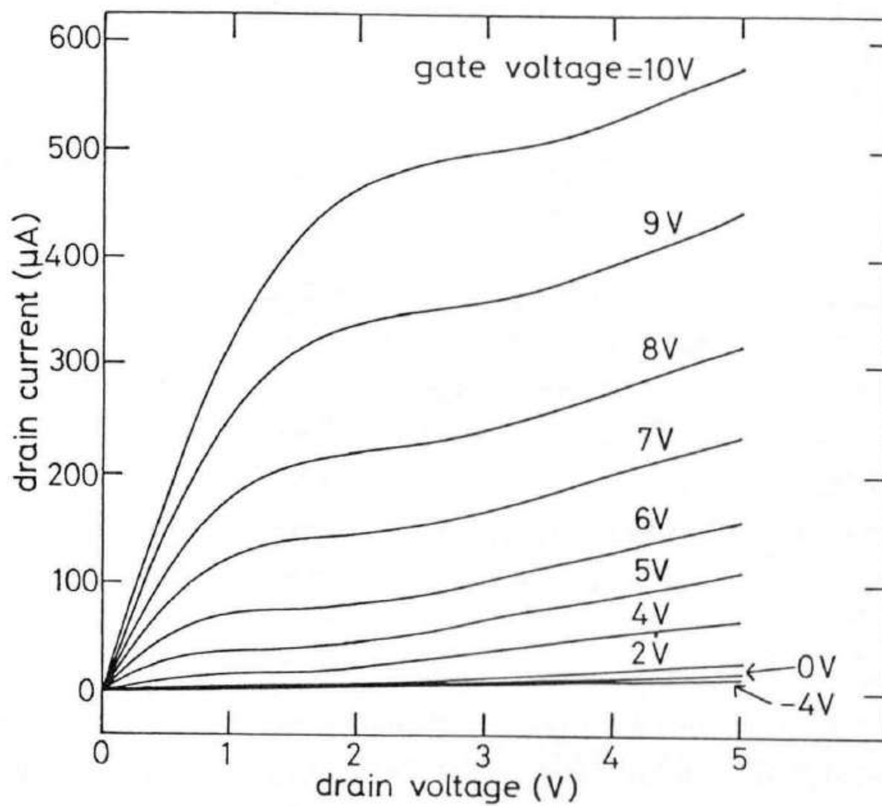

Fig. 10 Current-voltage characteristics of the MOSFET at 310K.

characteristics. The obtained effective electron mobility was about $100cm^2/Vsec$.

The measurement of I_d-V_d characteristics at high temperatures was attempted. The MOSFET whose characteristics are shown in Fig.10 did not operate at temperatures above 70°C because of breakdown of gate oxide. Simultaneously fabricated MOSFET's also showed the breakdown of the gate oxide by heating up to 100°C. Such breakdown phenomena are probably attributed to contamination during fabrication. Some other MOSFET's showed variation of I_d as a function of V_g up to 440°C. However, the gate oxide became leaky after heating up to 165°C and it did not recover after cooling. The observed worsening of gate insulation was considered to attributed to a reaction of Al and SiO_2. Au gate is effective to prevent such a problem[18]. To realize practical high temperature devices of 3C-SiC a combination of peripheral materials will be an important problem.

5. Summary

Ion implantation of P^+ and N_2^+ into p-type 3C-SiC was carried out. The annealing temperature dependence of electrical properties of implanted layers was investigated up to 1400°C. Electrical activation rates of implanted impurities were improved as annealing temperature became higher. N_2^+ implanted layers showed the larger electrical activation rate than P^+ implanted layers. P-n junction diodes were fabricated using an ion implantation technique. Their capacitance-voltage characteristics indicated that they had a p-i-n structure.

Inversion-type MOSFET's of 3C-SiC were fabricated. Source and drain were formed by the ion implantation of P^+. Inversion mode operation was confirmed for the first time. Current-voltage characteristics showed kinks in the saturation region which are known as a feature of SOI MOSFET's. Effective electron mobility in the MOSFET's was estimated to be about $100cm^2/Vs$. This successful fabrication of MOSFET's showed usefulness of the ion

implantation technique for device fabrication of 3C-SiC.

References

[1] R.B.Campbel and H.C.Chang, *Semiconductors and Semimetals* Vol.7 Part B, (Academic Press, New York, 1971) edited by R.K.Willardson and A.C.Beer, Chapter 9.

[2] O.J.Marsh, *Silicon Carbide-1973*, (University of South Carolina Press, Columbia, 1974) edited by R.C.Marshall, J.W.Faust, Jr. and C.E.Ryan., p.471.

[3] H.L.Dunlap and O.J.Marsh, Appl. Phys. Lett. 15(1969) 311.

[4] A.Addamiano, G.W.Anderson, J.Comas, H.L.Hughes and W.Lucke, J. Electrochem. Soc. 119(1972) 1355.

[5] V.M.Gusev, K.D.Demakov, M.G.Kosaganova, M.B.Reifman and V.G.Stolyarova, Sov. Phys. Semicond. 9(1976) 820.

[6] S.A.Belova, A.V.Vorob'ev, V.M.Gusev, K.D.Demakov, M.G.Kosaganova, N.K.Prokof'eva, M.B.Reifman, V.G.Stolyarova and V.A.Uzhegova, Sov. Phys. Semicond. 10(1976) 743.

[7] E.V.Kalinina, N.K.Prokof'eva, A.V.Suvorov, G.F.Kholuyanov and V.E.Chelnokov, Sov. Phys. Semicond. 12(1978) 1372.

[8] Y.Kondo, T.Takahashi, E.Sakuma and S.Misawa and H.Daimon, S.Yoshida and Y.Hayashi, Extended Abstr. of the 46th Autumn Meeting of the Japan Society of Applied Physics, Kyoto, October, 1985, 2p-C-11.

[9] H.Kong, H.J.Kim, J.A.Edmond, J.W.Palmour, J.Ryu, C.H.Carter, Jr., J.T.Glass and R.F.Davis, Material Society Symposia Proceedings vol.97, Anaheim, 1987(Material Research Society, Pittsburgh, 1987) p.232.

[10] H.Ryssel and I.Ruge, *Ion Implantation*, (John Wiley & Sons, Chichester, 1986), p.116.

[11] H.Ishiwara and S.Furukawa, Trans. IECE Japan 56-C(1973) 179, in Japanese.

[12] S.Furukawa, H.Matsumura and H.Ishiwara, Jpn. J. Appl. Phys. 11(1972) 134.

[13] J.E.Gibbons, W.S.Johnson and S.W.Mylroie, *Projected Range*

Statics, (Halsted Press, Stroudsburg, 1975) 2nd ed.

[14] H.Matsunami, *Handoutai-kougaku(Semiconductor Engineering)*, (Syoukoudou, Tokyo, 1983) p.139, in Japanese.

[15] K.Shibahara, S.Nishino and H.Matsunami, Jpn. J. Appl. Phys. 23(1984) L862.

[16] J.Tihanyi and H.Schleotterer, Solid-State Electron. 18(1975) 309.

[17] S.M.Sze, *Physics of Semiconductor Devices*, (John Wiley & Sons, New York, 1981) 2nd edition, Chapter 8.

[18] E.Sakuma, H.Daimon, M.Yamanaka, S.Misawa, K.Endo and S.Yoshida, Extended Abstr. of the 34th spring Meeting of the Japan Society of Applied Physics and of the related societies, Tokyo, March, 1987, 28p-W-9 and 28p-W-10.